Brush border spectrin is required for early endosome recycling in *Drosophila*

Matthew D. Phillips* and Claire M. Thomas‡

Departments of Biology, and of Biochemistry and Molecular Biology, The Pennsylvania State University, 208 Erwin W. Mueller Laboratory, University Park, PA 16802, USA

*Present address: Laboratory of Mammalian Genes and Development, NIH/NICHD, 6B Center Drive, Room 2B215, Bethesda, MD 20892, USA
‡Author for correspondence (e-mail: clairet@psu.edu)

Accepted 15 December 2005
Journal of Cell Science 119, 1361-1370 Published by The Company of Biologists 2006
doi:10.1242/jcs.02839

Summary

An apical brush border is a characteristic of many mature epithelia. This dynamic structure consists of dense microvilli supported by F-actin bundles that protrude into the apical cytoplasm, where they are crosslinked by spectrin and myosin II to form the terminal web. Little is known about the terminal web, through which vesicles transit to and from the apical membrane. Analysis of mutations in β_{Heavy}-spectrin, the *Drosophila* brush border spectrin, reveals that this protein is necessary for the maintenance of Rab5 endosomes in the midgut. As a consequence, an apical H^+ V-ATPase that is probably responsible for lumenal acidification is lost both from the brush border and Rab5 endosomes. Epistasis tests indicate that β_{Heavy}-spectrin is required during endocytosis after Dynamin and before Rab5-mediated endosome activities. These data are consistent with the location of spectrin in the terminal web, and suggest that this molecule is required for correct sorting decisions at the early endosome.

Supplementary material available online at
http://jcs.biologists.org/cgi/content/full/119/7/1361/DC1

Key words: Epithelium, Brush border, Spectrin, Rab GTPase, Endosome, *Drosophila*

Introduction

A brush border is characteristic of many mature transporting epithelia, and is conserved across vertebrate and invertebrate species (Bement and Mooseker, 1996; Bonfati et al., 1992). It can be divided into three subdomains: the microvilli, where active transport proteins reside; the exocytic/endocytic zone at the base of the microvilli, where protein delivery and recovery occur; and the terminal web in the apical cytoplasm, where the F-actin crosslinking proteins spectrin and non-muscle myosin II form a dense meshwork between the F-actin bundles protruding from each microvillus (Bement and Mooseker, 1996). Remarkably, whereas brush border components are rapidly turned over, this structure remains ordered and stable (Stidwill et al., 1984).

The development, structure and composition of the microvillar domain have been well characterized, and the delivery and operation of individual transporters and some cytoskeletal components are well understood (Bement and Mooseker, 1996). By contrast, very little is known about the function of the terminal web. This meshwork is an extremely dense and potentially formidable barrier to vesicle transport (Hirokawa et al., 1983b), and probably utilizes unique variations on exocytic and endocytic processes. For example, the close juxtaposition of a spectrin-based membrane skeleton (SBMS) to a membrane has long been thought to antagonize the endocytic machinery passively by excluding other coats, and proteolytic removal (Kamal et al., 1998) or network disassembly makes way for vesicle formation. However, the SBMS in the terminal web is not so closely juxtaposed to the membrane at the endocytic zone, suggesting that here it might not require removal to permit endocytosis. In addition, the high degree of order within the brush border cytoskeleton (Hirokawa et al., 1983a) makes is hard to envision how F-actin polymerization could assist in the initial departure of endocytic vesicles (Merrifield, 2004). Nonetheless, the dynamic nature of the brush border requires that vesicular transport across the terminal web must be vigorous, and many vesicles are seen in this region (Hirokawa et al., 1983a; Hirokawa et al., 1983b). It therefore seems likely that novel mechanisms of vesicle processing might exist in the terminal web. Vesicles are seen to associate with spectrin during their traverse (Hirokawa et al., 1983a), suggesting a role for spectrin in transport at the brush border.

Spectrins are rope-like cytoskeletal proteins largely comprising spectrin repeats of ~106 amino acids that form heterotetramers of α and β subunits; the *Drosophila* genome encodes a single α and two β subunits (β-spectrin and β_{Heavy}-spectrin; β_H). $(\alpha\beta)_2$- and $(\alpha\beta_H)_2$-spectrin are basolaterally and apically polarized, respectively. Several modular protein-protein and protein-lipid interaction motifs within each spectrin isoform confer specific functionalities upon these molecular scaffolds. Spectrins form two-dimensional networks, in conjunction with F-actin, that are associated with various membranes and have a wide array of cellular functions (Bennett and Baines, 2001; De Matteis and Morrow, 2000). Mutations in all non-erythroid spectrin genes examined to date cause substantial or complete lethality and pleiotropic phenotypes, demonstrating their essential role in cell structure (Bennett and Baines, 2001). However, the precise roles of most non-erythroid SBMS have yet to be fully defined.

Recently, we demonstrated that over-expression of the C-terminal domain of β_H in *Drosophila* salivary glands leads to

the sequestration of dynamin and the inhibition of endocytosis (Williams et al., 2004). These data suggest that the apical SBMS is interacting directly or indirectly with endocytic components and that the SBMS has an active role in protein turnover. We therefore sought to test the hypothesis that brush border spectrin is involved in endocytosis (Hirokawa et al., 1983a) by examining the role of fly β_H in protein turnover specifically in the terminal web of fly middle midgut. Several lines of evidence support the existence of a typical brush border organization in insects. In *Manduca sexta*, both biochemical and ultrastructural evidence support this notion (Bonfati et al., 1992). Similarly, in fly cells that have a well-developed brush border (Filshie et al., 1971), it is subtended by the apical SBMS (Thomas et al., 1998). Moreover, fly brush borders contain both unconventional myosin 1 isoforms typical of this structure: myosin IA in the terminal web, and myosin 1B in the microvilli (Morgan et al., 1995).

We now report that acid secretion and nuclear positioning in *Drosophila* cuprophilic cells (CCs) are dependent on the apical SBMS. Furthermore, we demonstrate that these cells contain defects in their early endosomes, and that loss of acid secretion is correlated with the dispersal of an apical H^+ V-type ATPase and Rab5 from both the apical membrane and the early endosome system. Genetic interaction experiments suggest that the SBMS is required for correct sorting decisions at the early endosome. These data demonstrate that apical spectrin in the terminal web has a role in establishing the level of brush border proteins through the regulation of the early endosome recycling pathway.

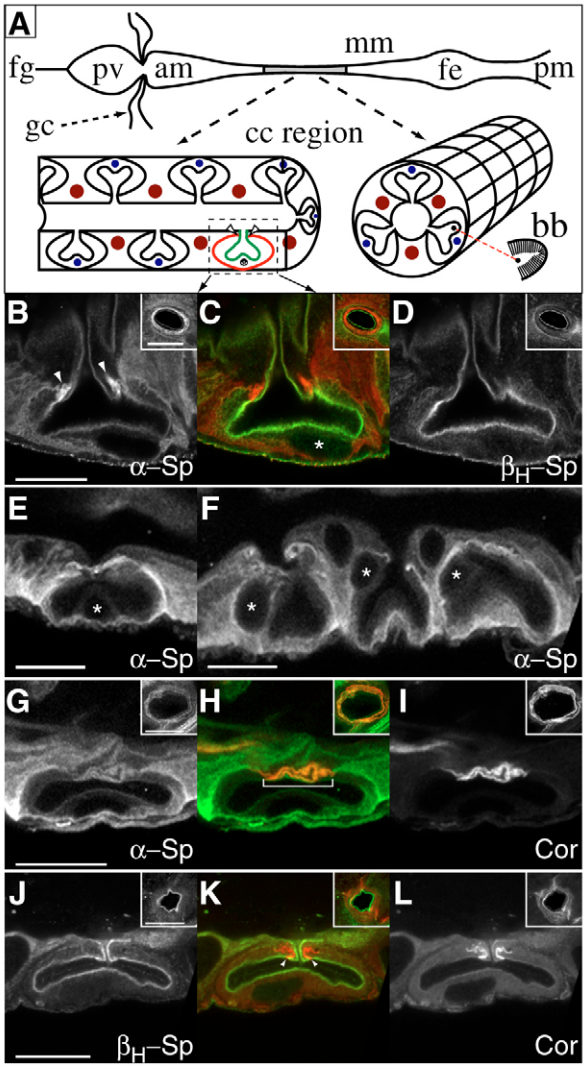

Fig. 1. β_H-spectrin distribution in middle midgut cells. (A) Top: schematic diagram of the larval middle midgut. fg, foregut; pv, proventriculus; gc, gastric caece; am, anterior midgut; cc, cuprophilic cell region; mm, middle midgut; fe, iron cell region; pm, posterior midgut; bb, brush border (illustrates how the long microvilli of the brush border almost fill the apical invagination). Bottom: diagrams illustrating sagittal section (left) and cross-section (right) through the cuprophilic cell (CC) region. For orientation, a dashed box surrounds a cell colored to resemble the staining in C. (B-D) Wild-type third-instar CCs co-stained for α-spectrin (B, α-Sp, red) and β_H-spectrin (D, β_H-Sp, green) and merged (C). β_H and α-spectrin co-label the terminal web subtending the apical surface. α is also present on the basolateral membrane and is concentrated at the septate junctions (B, arrowheads). Insets show a top-down view of the septate junction region of another cell. *, CC nucleus. (E,F) *karst* mutant third-instar cells stained for α-spectrin (α-Sp). α-spectrin is not present at the terminal web in the absence of β_H. The CC in (E) has a properly positioned nucleus (*), whereas the cells in (F) have mispositioned nuclei. Other examples of nuclear mislocalization are seen in Fig. 3J-L and Fig. 6C. (G-I) Parasaggital section of a wild-type third-instar CC co-labeled with α-spectrin (G, α-Sp, green) and septate junction marker Coracle (I, Cor, red). The merged image (H) shows co-localization at the highly folded junction (bracket). Insets are a top-down view of another septate junction. (J-L) Saggital section of a wild-type third-instar CC co-labeled with β_H-spectrin (J, green) and Coracle (L, red). The apical and basolateral domain abut at the apical margin of the junctions (arrowheads in K). Insets show a top-down view of another septate junction. Bars, 20 μm, except the inset in B, which is 10 μm.

Results

karst mutant CCs are polarized and exhibit a subset of α-spectrin mutant phenotypes

The *Drosophila* middle midgut CCs possess a deeply invaginated apical domain, with a prominent brush border (Fig. 1A). A pore connects the apical invagination to the gut lumen. (Fig. S1, supplementary material, contains a more detailed guide to the complex geometry of these cells that may aid the reader in interpreting the micrographs in this paper.) CCs are arranged along the middle midgut in a checkerboard pattern interspersed with the complementarily shaped interstitial cells. The CCs mark a region of intense gut acidification that disappears if the fate of the middle midgut cells is changed (Dubreuil et al., 2001). Since the midgut is a secondary epithelium, these cells have no zonula adherens and rely exclusively on smooth septate junctions (SJs) for lateral adhesion and as a barrier to permeability (see Filshie et al., 1971; Tepass, 1997).

As in other epithelia, β_H and α-spectrin co-localize at the apical domain of CC and interstitial cells, whereas β- and α-spectrin co-localize basolaterally (Fig. 1B-D) (Dubreuil et al., 2001; Dubreuil et al., 2000; Lee et al., 1993; Thomas et al., 1998). Additionally, α-spectrin is enriched in the SJ at the pore of the CC apical invagination (Fig. 1B-D, inset), where it co-localizes with the SJ marker Coracle (Fig. 1G-I, and insets). β_H abuts but does not overlap with Coracle (Fig. 1J-L, and

inset), identifying the apical margin of the SJ as the apical-lateral boundary in this cell type.

Previous analyses have shown that mutants for the common α-spectrin subunit have CCs with an enlarged pore and mispositioned nuclei, and exhibit an acidification defect in the middle midgut (Dubreuil et al., 1998; Lee et al., 1993). By contrast, mutants for basolateral β-spectrin exhibit only the enlarged pore phenotype (Dubreuil et al., 2000). Together, these results imply a role for the apical SBMS in nuclear positioning and gut acidification. We therefore examined *karst* mutant guts that lack wild-type β_H. Staining for α-spectrin in *karst* mutant guts confirms that α-spectrin is selectively lost from the apical membrane (Fig. 1E-F). This indicates that the *karst* mutation disrupts only the apical SBMS in this cell type, and supports earlier findings that $(\alpha\beta)_2$ tetramers do not substitute at the apical domain in the absence of β_H (see Zarnescu and Thomas, 1999). As predicted, we find that nuclei are often mispositioned in *karst* mutant CCs. Instead of their central wild-type location (Fig. 1E), 13-71% of the nuclei in each gut are found at the outer edges of the cell, causing a bulge near the pore (Fig. 1F). The variable expressivity of this phenotype suggests that $(\alpha\beta_H)_2$-spectrin has only an accessory role in nuclear positioning, or normally prevents stochastic shifts in position during gut peristalis and/or locomotion. We also find that gut acidification is defective in *karst* mutants (see below) but that CC pore sizes are normal. Together, these results show that the structural and functional defects caused by loss of the common α-spectrin are thus the sum of the disruption of the individual apical and basolateral SBMS.

Acid secretion by CCs requires the apical SBMS

Using Bromophenol Blue (BPB) as a pH indicator, it was shown that α-spectrin, but not β-spectrin, mutants lack the ability to acidify their guts (Dubreuil et al., 1998). Third-instar *karst* larvae were similarly fed BPB and a statistically significant decrease in overall acidification was apparent (Fig. S2, supplementary material). However, we found this assay to be susceptible to misinterpretation near the color transitions for BPB and ineffective at cellular resolution. Acridine Orange (AO), which undergoes a pH-dependent shift in emitted fluorescence, both provides a more consistent assay and is amenable to high-resolution microscopy. AO has been widely used as a marker of cellular compartments with a negative charge, such as lysosomes. Near neutral pH, light is primarily emitted at green wavelengths, but at an acidic pH the fluorescence is red-shifted.

In third-instar wild-type guts, red-shifted AO is found in the lumen and in the CC apical invaginations (Fig. 2A, arrows, and E), with the apical invaginations often exhibiting a greater red shift than the lumen. In individual CCs, we frequently see plumes of red-shifted fluorescence streaming out of the apical invagination into the gut lumen passing through a ring-shaped area of green fluorescence in the intersitial cells (Fig. 2A, arrowheads, B-D). The origin of this ring is unknown, but

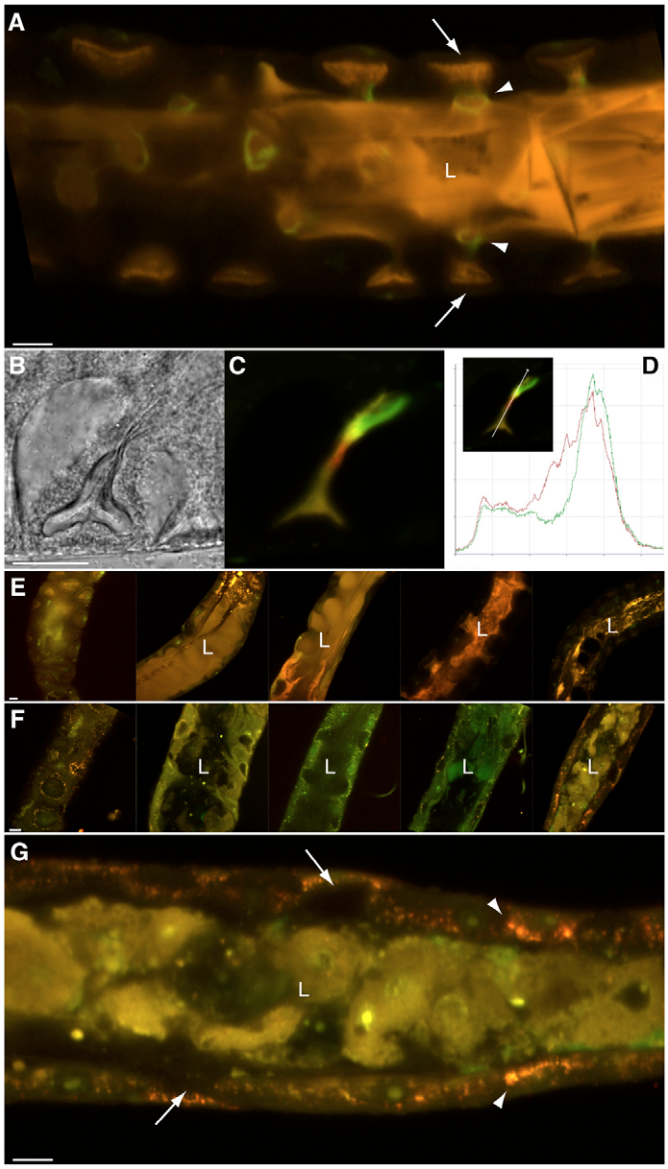

Fig. 2. Acridine Orange staining of third-instar intestines. (A) A segment of wild-type gut stained with AO. The CC apical invaginations (arrows) and gut lumen (L) are filled with a strongly red-shifted AO signal indicating robust acid production. The interstitial cells forming the pores also contain a ring of green fluorescence of unknown origin (arrowheads). (B-D) Wild-type third-instar CC; (B), brightfield view; (C), AO fluorescence. Parasagittal section showing red fluorescence in the apical invagination and pore, whereas the section intersects a green fluorescent ring in the interstitial cells. (D) Illustration of the efficacy of the AO probe by showing the relative red and green channel fluorescence along a transect in the cell in D (see inset). (E) Low-magnification views of representative wild-type guts stained with AO. All show a strongly red-shifted signal in the CC apical invaginations and gut lumen. The first panel is parasagittal, the rest are sagittal. L, lumen. (F) Low-magnification views of representative *karst* guts stained with AO. There is no AO signal from the CC apical invaginations, whereas the lumens are green to pale orange. Strong accumulation of red-shifted AO is seen in vesicular structures in mutant CCs. The first panel is parasagittal and the rest are sagittal. L, lumen. (G) Higher-magnification view of the segment of *karst* gut stained with AO in the rightmost panel in F, showing how the CC apical invaginations (arrows) are devoid of AO staining. The gut lumen is filled with mostly unshifted signal, indicating weak acidification. No green rings appear near the pores. Prominent red-shifted vesicles indicating low pH are visible in the CC cytoplasms (e.g. arrowheads). L, lumen. Bars, 20 μm.

appears to be an internal feature near the boundary of the intersititial cell and CC. Since the CC apical invaginations are the most acidic regions we observe, these data support the notion that they, and not interstitial cells, are the source of midgut acid.

AO staining in third-instar *karst* mutants reveals a consistent loss of acidification. The typical *karst* mutant gut lumen demonstrates very little, if any, red shift, indicating that the pH is significantly higher than in wild type (Fig. 2, compare A with G and E with F). The apical invaginations are typically devoid of fluorescence and acid plumes are no longer observed (Fig. 2G, arrows). These data indicate that the loss of acidification is associated with defects in the apical SBMS, and reinforce the hypothesis that the CC apical invagination is the source of acid for the midgut. In addition, there does not appear to be a ring of green fluorescence at the pore connecting the apical invagination and lumen, suggesting that either *karst* mutant interstitial cells are unable to produce it, or that this cell type only does so in response to acid secretion by adjacent CCs.

Staining with AO reveals an additional phenotype in *karst* mutant CCs. Faint acidic vesicles that are occasionally seen in wild-type cells are prominent and numerous in *karst* guts (Fig. 2G). This is suggestive of a defect in protein trafficking in *karst* mutants that leads to an increase in the number of lysosomes.

The H^+ V-type ATPase is mislocalized in *karst* mutant CCs

The proton pump responsible for midgut acidification has not yet been identified. However, the preeminent candidate is a H^+ V-type ATPase (V-ATPase), a multi-subunit complex thought to energize all insect epithelia (Wieczorek et al., 2000). In *Drosophila*, just one candidate V-ATPase exists in the genome, and has been localized to the apical membranes of Malpighian tubules, where it drives fluid secretion (Dow et al., 1994). We used the C23 antibody raised against *Manduca* V-ATPase subunit B (97% identical to *Drosophila* subunit B) (Dow, 1999) to localize the homologous fly protein. We confirmed that this antibody detects a single band of the predicted size in fly extracts (57 kDa, Fig. S3, supplementary material).

Immunofluorescent staining of wild-type third-instar *Drosophila* midguts with the V-ATPase antibody reveals apically concentrated staining at the base of the microvilli (Fig. 3C, arrows in I) and in large cytoplasmic concentrations that are found in both CC and interstitial cells (Fig. 3C, arrowheads in I). Staining is not seen in the microvilli because of the high density of pumps in the membrane, which excludes antibodies without antigen retrieval procedures (Wieczorek et al., 2000). In our hands, sufficient staining is seen for us to follow the fate of the pump at the apical membane. Apical membrane accumulation of this protein is not evident in interstitial cells, again consistent with the CCs being the source of acid. In *karst* mutants, the V-ATPase is undetectable at the apical surfaces of CCs, and is no longer found in a cytoplasmic compartment. Instead, only a diffuse cytoplasmic staining is seen (Fig. 3D-F, J-L). This perturbation indicates that the stability and/or subcellular location of this pump is dependent on an intact apical SBMS, and is consistent with this V-ATPase being the primary proton pump for gut acidification.

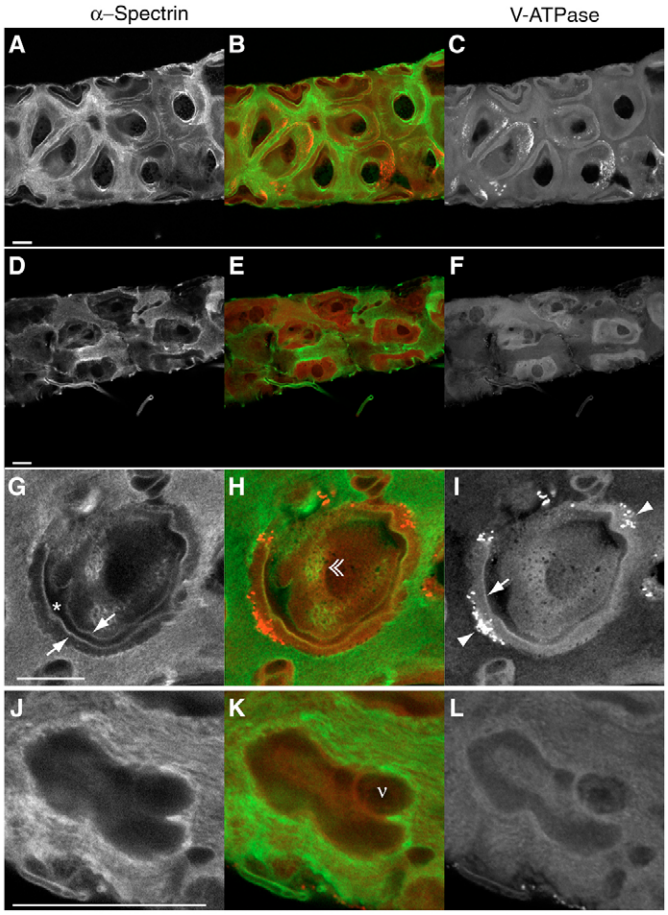

Fig. 3. V-ATPase staining of third-instar intestines. All samples were co-stained for α-spectrin (A,D,G,J) and V-ATPase (C,F,I,L). Panels B, E, H and K are merged images (α-spectrin in green, V-ATPase in red). (A-C) Wild-type gut. Cell shapes are revealed by α-spectrin, which outlines both the apical and basolateral domains and exhibits high cytoplasmic concentrations in the interstitial cell cytoplasm. CCs in the center present in cross-section as rounded shapes with the nucleus in the center; by contrast, cells on the top and bottom edges of the gut are parasagittal with a cup-shaped apical invagination around the nucleus. The V-ATPase signal is visible at the apical domain and in clustered vesicular structures. (D-F) *karst* mutant gut. α-spectrin stains only the basolateral membranes in the absence of β_H. V-ATPase staining is diffusely cytoplasmic, lacking both apical and vesicular concentrations. (G-I) Vertical cross-section of an individual wild-type CC. α-spectrin stains both basolateral membrane and the terminal web (G, arrows) on either side of the apical invagination (G, asterisk). The terminal web in the center of the cell runs parallel to the image plane and dips into focus near the nucleus where again elevated V-ATPase can be seen (chevron in H). V-ATPase co-localizes with α-spectrin in the terminal web at this resolution (H, arrow in I), and is also seen in numerous cytoplasmic vesicles near the basal membrane (H, arrowheads in I). (J-L) Vertical cross-section of an individual *karst* mutant CC. α-spectrin stains the basolateral membrane only in this cell. The V-ATPase signal is diffuse and cytoplasmic, demonstrating neither an apical accumulation nor a vesicular concentration. Note also the misplaced nucleus (*v* in K). This view is in a similar plane to that illustrated in Fig. S1D (supplementary material). Bars, 20 μm.

The early endosome is disrupted in *karst* mutants

In order to determine the nature of the V-ATPase-containing compartments, we performed immunofluorescent co-localizations for V-ATPase and markers of various intracellular

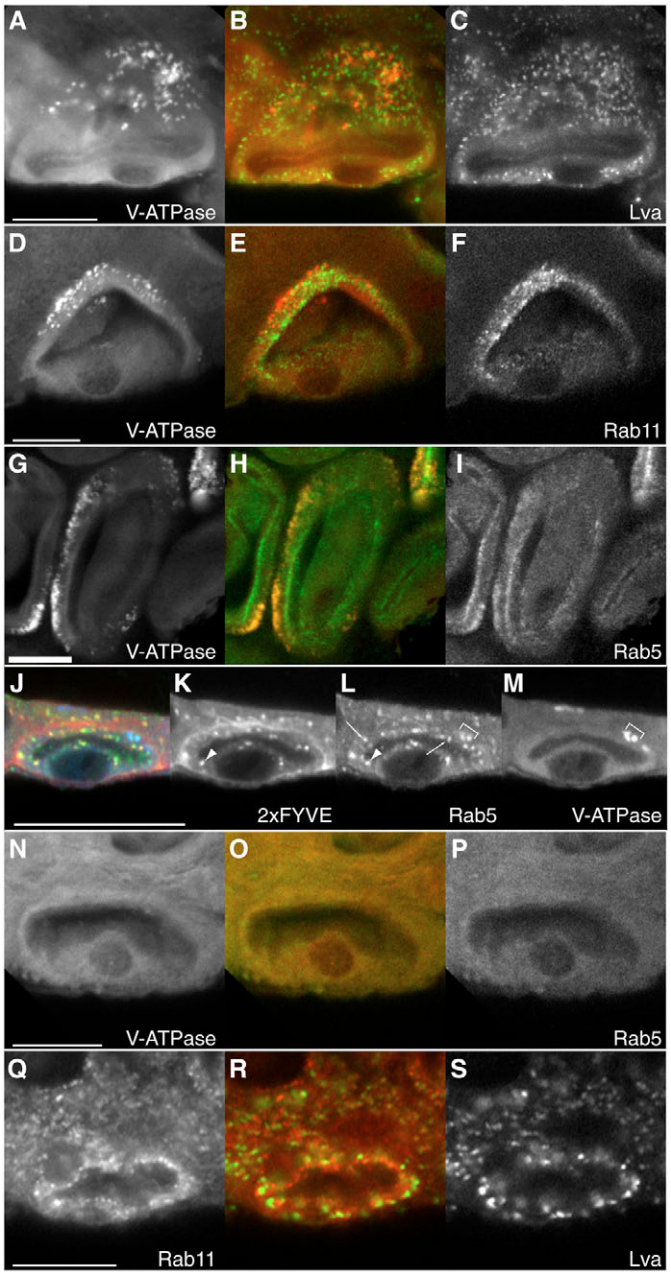

Fig. 4. V-ATPase is located in a subset of Rab5-positive endosomes in CCs. Cells shown are all from third-instar guts except where noted; 'red' and 'green' refer to colors in the central merged image. (A-C) Wild-type cell stained for V-ATPase (A, red) and the Golgi marker Lava Lamp (C, Lva, green). No co-localization is evident. (D-F) Wild-type cell stained for V-ATPase (D, red) and the recycling endosome marker Rab11 (F, green). No co-localization is evident. (G-I) Wild-type cell stained for V-ATPase (G, red) and the early endosome marker Rab5 (I, green), showing that all V-ATPase-positive structures co-label for Rab5. However, not all Rab5-positive endosomes co-label for V-ATPase. (J-M) A myc-2xFYVE construct was expressed in first-instar larval CCs to label phosphatidylinositol 3-phosphate [PtdIns(3)*P*]-positive endosomes. These were stained for Myc (K/2xFYVE, red), Rab5 (L, green) and V-ATPase (M, blue). Three classes of early endosomes are revealed: those labeled with Rab5 alone (e.g. arrows in L), those co-labeled with Rab5 and myc-2xFYVE (e.g. arrowhead in K and L), or those labeled with Rab5 and V-ATPase (bracket in L and M). Also, myc-2xFYVE stains the basolateral but not the apical membrane. (N-P) *karst* mutant cell stained for V-ATPase (N, red) and Rab5 (P, green). Not only is the V-ATPase dispersed but none of the Rab5-positive compartments are evident. (Q-S) *karst* mutant cell stained for Rab11 (Q, red) and Lava Lamp (S, Lva, green), showing that recycling endosomes and Golgi are intact and indistinguishable from wild type in the absence of β_H-spectrin. Bars, 20 μm.

compartments. Neither Lava Lamp, a Golgi marker (Sisson et al., 2000), nor Rab11, a marker of the recycling endosome (see Jankovics et al., 2001, and references therein), co-localizes with the V-ATPase-labeled cytoplasmic compartment (Fig. 4A-C, D-F, respectively), although Rab11 does exhibit a partial overlap with the V-ATPase in the terminal web region. However, Rab5, an early endosome marker (Wucherpfennig et al., 2003), co-labels the V-ATPase-positive compartment (Fig. 4G-I). Rab5 is also found at the apical surface and in several smaller vesicular structures, consistent with its known roles in endocytosis and recycling.

To refine further the identity of the Rab5-positive endosomal compartments, we performed an additional immunolabeling experiment using larvae expressing the UAS-2xFYVE transgene using the *mex-GAL4* driver, which expresses GAL4 in first- and second-instar middle midgut. The 2xFYVE protein is a widely used marker that specifically labels phosphatidylinositol 3-phosphate [PtdIns(3)*P*]-positive early endosomes, reflecting the activation of phosphoinositide 3-kinase (PI 3-kinase) by Rab5 (Wucherpfennig et al., 2003). This experiment further subdivides the CC early endosomes into three populations of Rab5-positive compartments: (1) those with Rab5 alone found near the apical membrane; (2) those co-labeling with Rab5 and 2xFYVE found in the cytoplasm; and (3) those with Rab5 and the V-ATPase found near the basal membrane at the pore (Fig. 4J-M). No triple labeling of any single compartment was observed. These data indicate that a major pool of the V-ATPase resides in an early endosomal compartment that is PtdIns(3)*P* negative. An additional observation is the labeling of the entire basolateral membrane by the 2xFYVE construct whereas it is not detected at the apical domain. Such an absolute segregation of a membrane lipid along the apicobasal axis has, to our knowledge, not been documented before.

The presence of V-ATPase in a Rab5-positive endosome suggests that this represents a pool of the pump that is recycling from the apical membrane. To test this hypothesis, we examined the distribution of the V-ATPase in a temperature-sensitive *Shibire*^{2Ts} (*Shi*^{2Ts}) background where dynamin can be inactivated by raising the temperature of the larvae. After 1 hour at the non-permissive temperature, we found that both Rab5 and V-ATPase strongly accumulated at the apical membrane (see Fig. 6, compare A,B with E,G). This demonstrates that the pump is actively internalizing and that dynamin is not required for its delivery to the apical membrane. In addition, the intensity of Rab5 staining at the V-ATPase-positive endosomes is noticeably decreased (Fig. 6E-G, insets), suggesting that the inactivation of dynamin decreases the movement of Rab5 to this compartment, consistent with the notion that the pump is recycling from the apical membrane to this location.

In *karst* mutant third-instar larvae, the endosomal structures that stain for V-ATPase are lacking. To determine

if this compartment is still present, Rab5 antibodies were used to stain *karst* mutant third-instar midguts. This revealed that no structures corresponding to Rab5-positive endosomes are detectable in any mutant cells. Instead, only low-level diffuse cytoplasmic staining of Rab5 is seen, resembling the mis-distributed V-ATPase (Fig. 4N-P). By contrast, Lva and Rab11 distributions appear normal in *karst* guts (Fig. 4Q-S).

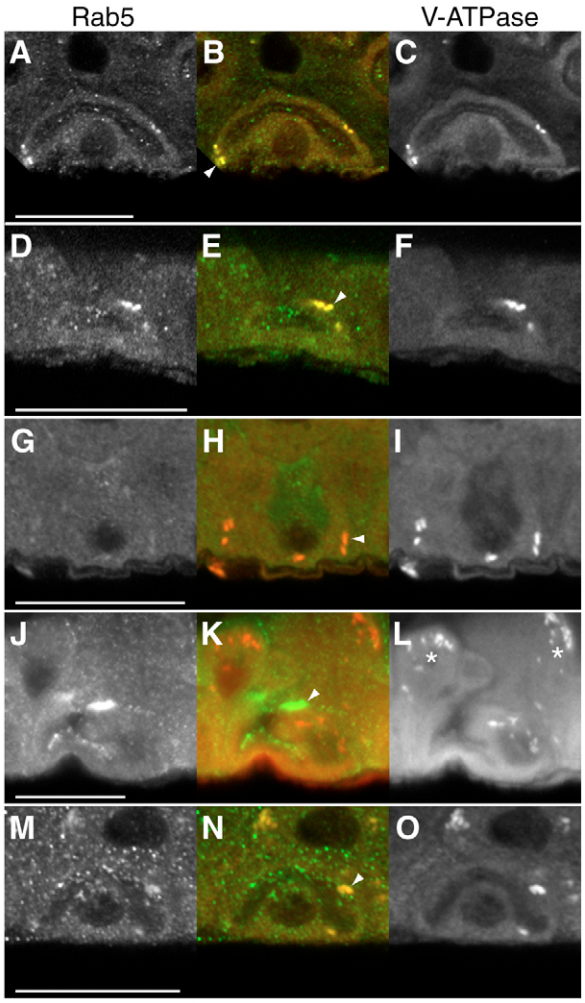

Fig. 5. Lack of β_H prevents dominant-negative Rab5 disruption of the early endosome. All cells are from first-instar guts except (J-L), which are from second-instar guts. Staining is for Rab5 (A,D,G,J,M, green in merge) and V-ATPase (C,F,I,L,O, red in merge). (A-C) Wild-type CC co-stained for Rab5 and V-ATPase, showing co-localization (arrowhead). (D-F) *karst* mutant CC co-stained for Rab5 and V-ATPase. At this stage, Rab5 endosomes appear intact and V-ATPase co-labels as in wild type (arrowhead). (G-I) Expression of Rab5S43N in wild-type CCs virtually eliminates the Rab5 signal at V-ATPase-positive endosomes (e.g. arrowhead) and eliminates the typical particulate Rab5 pattern. (J-L) By the second instar, wild-type CCs expressing Rab5S43N show non-overlapping distributions of Rab5 and V-ATPase. Rab5 is invariably concentrated adjacent to the septate junctions near the pore (arrowhead), whereas the V-ATPase is often seen in multiple compartments, especially in the apical cytoplasm of interstitial cells (L, asterisks). (M-O) Expression of Rab5S43N in *karst* mutant CCs fails to reduce the Rab5 signal at V-ATPase-positive endosomes (e.g. arrowhead) and does not eliminate the typical particulate Rab5 staining pattern. Identical results are seen in second-instar guts that still contain V-ATPase-positive endosomes (complete data set is shown in Fig. S4, supplementary material), except as noted in (J-L) above. Bars, 20 μm.

To examine the etiology of this phenotype, we examined earlier larval stages. Staining *karst* mutant first-instar larvae with Rab5 and V-ATPase antibodies reveals an intact early endosome (Fig. 5, compare A-C with D-F). Moreover, AO feeding experiments indicate that the lumen is acidified in both wild-type and *karst* mutant guts at this stage (M.D.P. and C.M.T., unpublished data). In the second instar, the Rab5 compartment has disappeared in some of the *karst* mutant guts, although the majority still display a near wild-type appearance (Fig. S4, supplementary material, compare A-C with D-F). Together, these data indicate that *karst* midgut cells contain a selective defect in their recycling pathway that leads to the loss of early endosomes around the transition from second to third instar.

The loss of the early endosome in *karst* mutant cells is reminiscent of the phenotype induced in neurons by expressing a dominant-negative Rab5 (Rab5S43N), which is constitutively bound to GDP (Wucherpfennig et al., 2003). Using the *mex-GAL4* driver line, we expressed Rab5S43N in the midgut. This induced a marked loss of Rab5 from V-ATPase-labeled endosomes in both CC and interstitial cells in the first instar (Fig. 5G-I). By the second instar, the V-ATPase and Rab5 no longer co-localize (Fig. 5J-L). However, V-ATPase-labeled structures remain prominent both in CCs and in interstitial cells, whereas the Rab5 antibody now labels a distinct compartment near the CC pore. This continued presence of a Rab5-labeled compartment upon expressing Rab5S43N in the first-instar larval midgut differs from its effects in the fly nervous system, where a total loss of particulate Rab5 staining was observed, suggesting the disintegration of the early endosome (Wucherpfennig et al., 2003). This might result either from differing levels of expression from the different drivers or from tissue-specific responses. Although Rab5 is thought to have roles in both the formation of endocytic vesicles and their fusion at the early endosome (Pfeffer, 2003), we do not observe an accumulation of V-ATPase at the apical membrane when Rab5S43N is expressed in wild-type cells. Thus, our results suggest that Rab5-mediated events at the early endosome are most sensitive to inhibition in this tissue.

In order to test whether β_H and Rab5 operate in the same pathway, we expressed Rab5S43N in a *karst* mutant background and examined early larval stages where *karst*-induced loss of Rab5 has not yet occurred. Strikingly, the loss of β_H prevents Rab5S43N-induced dissociation of Rab5 from the V-ATPase-labeled compartment in both first and second-instar larvae (Fig. 5M-O and Fig. S4J-L, supplementary material, respectively). This epistatic relationship strongly suggests that Rab5 and β_H operate in a common pathway that is required for endosomal integrity but that β_H is upstream of Rab5 and that the *karst* mutation limits the loss of endosomal identity induced by Rab5S43N.

To determine more precisely the stage at which β_H-spectrin functions in the recycling pathway, the Shi^{2Ts} allele was employed to inhibit endocytosis. In third-instar Shi^{2Ts}/Y larvae at the permissive temperature, the distribution of Rab5 and V-ATPase appears normal (Fig. 6A-B); whereas Rab5 puncta and

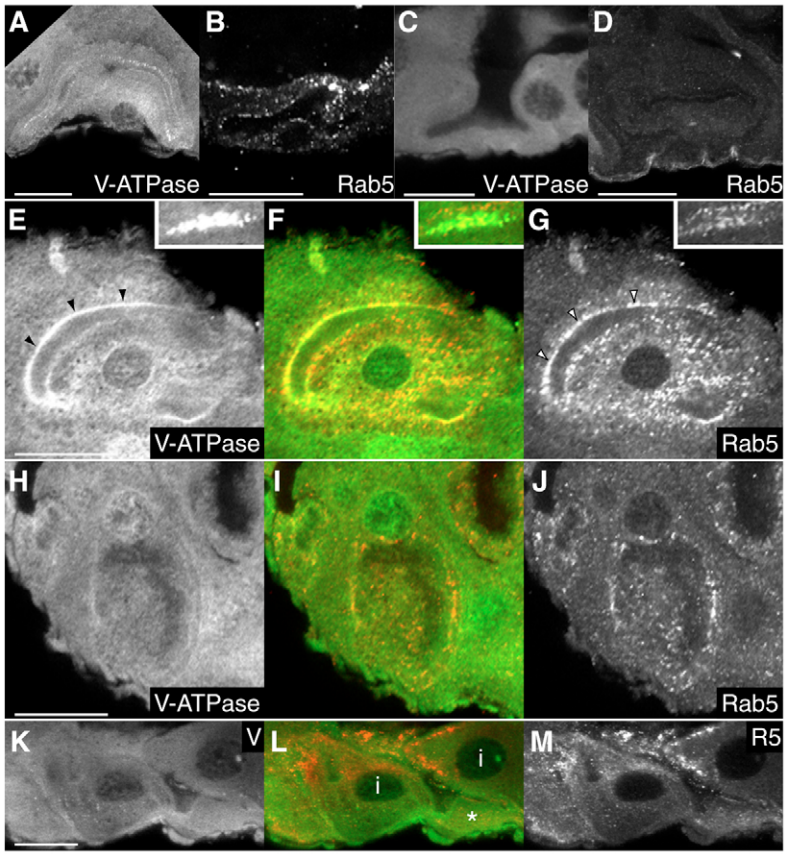

Fig. 6. Apical delivery of V-ATPase continues in *karst* mutant cells. All CCs shown are from third-instar guts; 'red' and 'green' refer to colors in the central merged image. (A) Staining for V-ATPase in a *Shibire*^{2Ts} (*Shi*^{2Ts}) mutant cell at the permissive temperature reveals a normal endosomal and apical localization (see Fig. 4G). (B) Staining for Rab5 in a *Shi*^{2Ts} cell at the permissive temperature reveals a normal distribution (see Fig. 4I). (C) Staining for V-ATPase in a *Shi*^{2Ts}/*karst* double-mutant cell at the permissive temperature reveals only the diffuse cytoplasmic staining characteristic for *karst* mutants. (D) Staining for Rab5 in a *Shi*^{2Ts}/*karst* double-mutant cell at the permissive temperature reveals only the diffuse cytoplasmic staining characteristic for *karst* mutants. (E-G) Staining for V-ATPase (E, red) and Rab5 (G, green) in a *Shi*^{2Ts} mutant cell at the restrictive temperature reveals a strong apical accumulation for both proteins (arrowheads). The inset shows a co-labeled endosomal compartment from another cell. Here, Rab5 is still present, but the signal appears weaker and somewhat patchy compared with the permissive temperature. (H-M) Staining for V-ATPase (H,K: V, red) and Rab5 (J,M: R5, green) in *Shi*^{2Ts}/*karst* double-mutant cells at the restrictive temperature. Both proteins co-accumulate at the apical membrane of CCs (H-J), although V-ATPase is weaker and is variable from larvae to larvae. No V-ATPase- or Rab5-positive endosomes are evident. Rab5 particles also accumulate near the apical membrane in interstitial cells (i), with no evident V-ATPase staining (K-M). Asterisk indicates a CC with apical Rab5 accumulation, but very weak V-ATPase accumulation. Bars, 20 μm.

a broad band of V-ATPase signal became concentrated at the apical membrane at the restrictive temperature (Fig. 6E-G). In addition, Rab5 staining at the V-ATPase-labeled endosome is reduced (compare insets in Fig. 6E,G with Fig. 4G,I), indicating it is not being replenished.

The Rab5 and V-ATPase staining patterns in third-instar *Shi*^{2Ts}/*karst* double-mutant larvae (*Shi*^{2Ts}/*Y; kst*^{2}/*Df(3L)1226*) at the permissive temperature are identical to *karst* mutants – weak and diffusely cytoplasmic with no endosomal concentration (Fig. 6C-D; compare with Fig. 3 and Fig. 4N-P). At the restrictive temperature, Rab5 reappears in numerous cytoplasmic puncta with a strong accumulation near the apical membrane, particularly in the interstitial cells (Fig. 6J,M). Also at the restrictive temperature, the V-ATPase staining sometimes becomes concentrated at the apical domain, but remains diffuse in most cells (Fig. 6H). A lower level of apical pump accumulation is to be expected in the *karst* mutant background, since the endosomal pool is gone and its delivery is presumably dependent on de novo synthesis of protein. These data indicate that we are achieving a significant inhibition of endocytosis. In cells that have accumulated apical V-ATPase, it does not co-localize with any Rab5-positive vesicles, and no staining typical of the large V-ATPase-positive endosome is evident (Fig. 6H-J). Thus, *Shi*^{2Ts} is epistatic to *karst* at the plasma membrane. Together with the previous experiment combining *karst* and Rab5S43N, our results are fully consistent with a role for β_H after dynamin pinches off endocytic vesicles but before Rab5-mediated endosome fusion occurs.

Discussion

Here, we demonstrate that β_H-spectrin in the terminal web has a role in Rab5-mediated endosomal recycling. Specifically, we report that *karst* mutant cells of the *Drosophila* midgut specifically lose all Rab5-positive endosomes at around the transition from second to third instar, whereas other endomembrane compartments remain intact. This defect results in the loss of functional H^+ V-ATPase from the apical membrane and a failure to acidify the larval gut lumen. This phenotype correlates with an increase in the number of Acridine Orange (AO)-accumulating acidic vesicles, suggesting that late endosomes/lysosomes become more numerous, and that recycling/degradation decision-making is disrupted in the absence of spectrin. This is the first function ascribed to spectrin in the brush border, and represents a novel role for the F-actin cytoskeleton during endocytosis that might be a functional specialization of brush border organization.

Polarization of the membrane skeleton reflects specialized roles

In primary epithelia $(\alpha\beta)_2$- and $(\alpha\beta_H)_2$-spectrin are basolateral and apical, respectively, and this characteristic distribution is also evident in the midgut (Fig. 1B-D) (Dubreuil et al., 2000). Here, detailed examination of loss-of-function mutations was performed in these cells for all three spectrin loci and we conclude that the apical and basolateral SBMS have distinct and separable functions. Thus, mutation of the common α-spectrin chain causes defects in nuclear positioning, acid secretion and pore size (Dubreuil et al., 1998; Lee et al., 1993). Defects in pore size and Na^+K^+ ATPase localization have been

ascribed to basolateral β-spectrin (Dubreuil et al., 2000), whereas defects in nuclear localization and acid secretion arise from loss of apical β_H-spectrin (shown here). In agreement with previous studies in primary epithelia (Zarnescu and Thomas, 1999), apical spectrin is not required to establish the apicobasal axis and no evidence of redundancy between the two SBMS is evident.

β_H-spectrin is required for acid secretion

Drosophila CCs define a region of intense gut acidification. Several lines of evidence indicate that it is this cell type that secretes protons. First, our observations that AO accumulates in the lumen of the CCs and is most protonated in the pores exiting these cells (Fig. 2A-D) provides direct evidence that this cell type is responsible acidification of the lumen. Second, proton-secreting cells in insect epithelia are energized by a H^+ V-type ATPase (V-ATPase) located at their apical surface (Wieczorek et al., 2000), and we have localized the *Drosophila* V-ATPase to the apical surface of CCs (Fig. 3C,I), but not the interstitial cells. Furthermore, in *karst* CCs, where the gut lumen is no longer acidified (Fig. 2F,G, Fig. S2, supplementary material), this V-ATPase is no longer detected at the apical membrane (Fig. 3F,L) and AO no longer accumulates in their apical invaginations (Fig. 2F-G), correlating the presence of this pump with proton secretion. These data are supported by reports demonstrating that gut acidification is dependent upon the differentiation of the CC and interstitial cell region (Dubreuil et al., 2001), and that the development of a deeply invaginated apical domain in CCs is characteristic of oxyntic cells from other animal systems (Dow, 1992; Forte and Yao, 1996).

An additional reservoir of V-ATPase is seen in a subset of the Rab5-positive endosomes that do not contain PtdIns(3)*P* (Fig. 4J-M). The apical enrichment of V-ATPase when dynamin is inhibited (Fig. 6E-F) indicates that this pump is actively recycling. This situation is reminiscent of pumps found in some vertebrate cells (e.g. Forte and Yao, 1996; Pastor-Soler et al., 2003), where V-ATPases also recycle between internal compartments and the apical membrane. Definitive evidence that this is indeed the V-ATPase responsible for acid secretion must await future analyses. Nonetheless, this pump serves as a useful maker to assess the effects of *karst* mutants on the endomembrane system.

β_H-spectrin regulates protein recycling through the early endosome

karst mutant midgut cells accumulate numerous and prominent AO-labeled compartments (Fig. 2G). These vesicles are often red-shifted, which is indicative of a low pH and thus the presence of more-numerous late endosomes or lysosomes. This suggests that loss of $(\alpha\beta_H)_2$-spectrin has consequences for membrane trafficking outside of the terminal web region. This is further corroborated by the observation that *karst* mutant cells in third-instar larvae not only lack V-ATPase at the apical membrane but also the endosomal pool of this enzyme and any detectable Rab5-positive cytoplasmic compartments (Fig. 4N-P). This extensive perturbation of Rab5 endosomes is highly selective since markers for recycling endosomes (Rab11) and the Golgi apparatus (Lava Lamp) are still present in a wild-type distribution (Fig. 4Q-S). The loss of Rab5-positive compartments appears to occur around the transition from the second to third instar, since Rab5 and V-ATPase exhibit a normal distribution in first-instar larvae (Fig. 5, compare A-C with D-F), are sometimes absent in (presumably late) second-instar larvae and are uniformly absent by the third instar (Fig. 4N-P). This timing correlates with the onset of a major growth phase during which the third-instar larva will more than quadruple its mass (Ashburner, 1989). The cells of the gut also grow to accommodate this increase in size and we speculate that the run down of the recycling system in *karst* mutants at this time results from an underlying weakness in endosome dynamics coupled with this rapid growth, rather than a complete block in one step. This effect cannot be the result of maternal perdurance, because the interaction between the *karst* mutation and dominant-negative Rab5 activity reveals this defect during the first instar (see below).

The selective perturbation of one intracellular trafficking pathway arising from the loss of spectrin in the terminal web is not an obvious prediction from its location (Hirokawa et al., 1983a). However, the results of the epistasis experiments are consistent with this position between the apical membrane and the endosome (Fig. 7). In *karst* mutant third-instar larvae, the apical accumulation of Rab5 and sometimes V-ATPase when dynamin is inhibited (Fig. 6H-J) demonstrates that β_H is not required for the delivery of V-ATPase or the recruitment of Rab5 during endocytosis, and places spectrin function downstream of initial internalization events. This result also indicates that Rab5 is still present in the cells in the absence of β_H. However, in first- and second-instar *karst* mutant larvae, Rab5S43N disruption of Rab5 localization to endosomes is

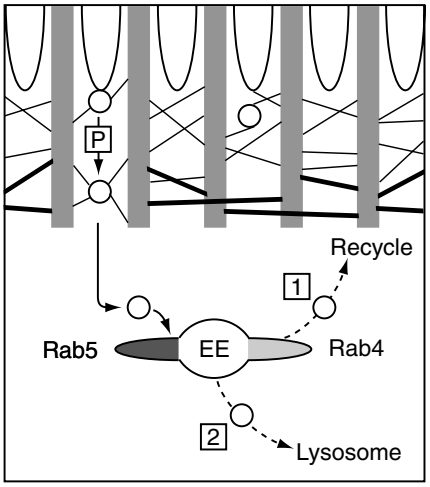

Fig. 7. A model for the role of brush-border spectrin in the recycling pathway. Newly formed endocytic vesicles must navigate through the F-actin rootlets (gray vertical bars), spectrin (thin black filaments) and myosin II (thick black strands) in the terminal web before proceeding to the early endosome (EE), where a decision is made either to return the protein to the membrane (recycle, 1) or to follow the degradation pathway (lysosome, 2). Our data suggest that brush border spectrin 'primes' proteins on vesicles in the terminal web (P) in a way that influences the decision to recycle or degrade them at the early endosome. In β_H-spectrin mutants, we suggest that diversion of membrane flow along pathway 2 results in the run down of the early endosome system at the start of the third instar and the concomitant increase in lysosomal compartments that we observe.

abrogated. This places β_H function upstream of vesicle fusion and/or other events at the early endosome. Although it remains possible that β_H resides undetected at the early endosome, it is striking that our data reflect the location of spectrin in the terminal web in relation to the exit of newly internalized vesicles – between the microvilli where dynamin pinches off vesicles, but above the apical cytoplasm where Rab5 must be active for endosome fusion. Immunolocalization of spectrin in the mouse terminal web in quick-freeze deep-etch specimens reveals numerous examples of contact with newly endocytosed vesicles (Hirokawa et al., 1983a), an observation that is also consistent with this hypothesis.

The early endosomal system is a dynamic network of sorting organelles that is maintained by localized activation of specific Rab GTPases and requires cooperative interactions within and between its constituent domains (Seabra and Wasmeier, 2004). Thus, a wholesale redirection of the sorting process would have severe consequences for endosomal maintenance. The epistatic relationship of β_H, dynamin and Rab5 mutations, together with the superabundance of acidic vesicles in *karst* mutant cells that indicates increased lysosomal trafficking, suggest the hypothesis that brush border spectrin 'processes' newly internalized proteins to make them competent to enter the recycling pathway at the early endosome (Fig. 7). Thus, in the absence of spectrin, the diversion of large quantities of protein and membrane to the lysosomal pathway, coupled with the interlinked nature of the endosomal system, would result in the run down of the entire Rab5 network. An attractive hypothesis in this scenario that would satisfy the observed location of spectrin in the terminal web, yet the effects of its loss are seen at the endosome, is that spectrin might be important for polarizing activities that modulate the ubiquitylation state of freshly internalized proteins (Raiborg et al., 2003).

Materials and Methods

Fly stocks

karst alleles have been previously described (Thomas et al., 1998; Zarnescu and Thomas, 1999). Wild-type controls utilized either Oregon-R or the *karst* progenitor line *mwh ve red*. The midgut UAS driver P{w^{+mC} GAL4::Hsp70Bb$^{mex.P5'2.1}$=mexGAL4} was created as follows: a 2.1 kb promoter fragment from the *mex1* locus (a gift from S. Newfeld, Arizona State University, Tempe, AZ) was excised with *Eco*R1 and *Kpn*1 and inserted into pGaTB upstream of the *GAL4* gene. The *mex-GAL4* cassette was then subcloned into pP{CaSpeR-4} using *Kpn*1 and *Not*1, the sequence was verified and used to transform *yw; Sb Δ2-3*/TM6, *Ubx* according to standard methods (Rubin and Spradling, 1982). This driver expresses *GAL4* from late embryogenesis through the second instar in the middle midgut, reflecting regulation of the *mex1* gene (Newfeld et al., 1996). P{Rab5$^{S43N.Scer\UAS}$=UAS-*Rab5.S43N*} (dominant-negative Rab5) was a gift from M. Gonzalez-Gaitan (Max-Planck-Institut, Dresden, Germany). The temperature-sensitive *Shibire^{2Ts}* (Dynamin) line was acquired from the *Drosophila* stock center (Bloomington, IN). Recombinant *kst^2* UAS-D*Rab5^{S43N}/TM6B* and *Shi^{2Ts}; Df(3L)1226/TM6* lines were generated using standard genetic methods.

Dye feeding experiments

Bromophenol Blue (BPB; 0.2% w/v) was added to freshly made yeast paste (2.78 g instant yeast, 8 ml dH_2O). Up to 40 third-instar larvae were fed this yeast paste for ⩾2 hours before observation. The recessive marker *red* on the *karst* chromosomes was used to identify mutant larvae. Larvae that had filled their guts with dye were dissected in 1× PBS containing 5 mM EGTA to paralyze continuing peristaltic motions of the intestine, facilitating rapid observation and preventing the mixing of gut contents and rupture. Observations on each live gut were made immediately during each dissection. Our titration experiments for BPB are: yellow/green/blue at pH 1.8/1.8-3.0/3.0, respectively.

Acridine Orange (AO; 100 μM) was fed to larvae in a solution of 10% sucrose 30 to 60 minutes before dissection as above, and immediately observed. AO imaging was carried out using a Zeiss LSM 510 META confocal microscope (Carl Zeiss) with a 488 nm laser line. Unshifted and acid-shifted fluorescence was detected using 500-530 nm and 565-615 nm filters, respectively. To facilitate comparison, both wild-type and *karst* mutant larvae were always examined in each session using the same 40× water immersion lens and identical microscope settings.

Antibodies

All antibodies were raised against *Drosophila* proteins unless otherwise stated, and were used at the following concentrations: mouse monoclonal anti-human-Myc (Ab-1, clone 9E10; Oncogene Research Products) and rabbit anti-β_H (#243) (Thomas and Kiehart, 1994) were used at 1:300. Mouse anti-Coracle (from R. Fehon, University of Chicago, Chicago, IL) was used at 1:50. Mouse anti-α-spectrin (ascites #N3; from D. Branton, Harvard University, Cambridge, MA) was used at 1:600. Guinea-pig anti-*Manduca* V-ATPase subunit B (#C23; from M. Huss, University of Osnabruck, Osnabruck, Germany) was used at 1:150 for immunofluorescence and 1:1500 on immunoblots. Rabbit anti-Lava Lamp (from J. Sisson, University of Texas, Austin, TX) was used at 1:5000, rat anti-Rab11 (from R. Cohen, University of Kansas, Lawrence, KS) was used at 1:1000, and rabbit anti-Rab5 (MP1; from M. Gonzales-Gaitan, Max-Planck-Institut, Dresden, Germany) was used at 1:75. For secondary antibodies: Alexa Fluor 546 goat anti-mouse and Alexa Fluor 488 goat anti-rabbit antibodies (Molecular Probes) were used at 1:250. Cy5 goat anti-guinea-pig, Cy3 goat anti-rat, and FITC goat anti-mouse antibodies (Jackson ImmunoResearch) were used at 1:250. HRP-conjugated anti-guinea-pig antibodies (Sigma-Aldrich) were used at 1:2000.

Immunofluorescence and immunoblots

Larvae were dissected in fresh 4% paraformaldehyde in 1× PBS, and incubated for 20-45 minutes with rocking at room temperature. Hemizygous temperature-sensitive *Shi^{2Ts}* third-instar larvae were submerged in vials in a 34°C water bath for 1-2 hours immediately prior to dissection. Third-instar middle midguts were dissected away from the rest of the intestine for better antibody penetration. For all intestines, fixation was followed by three washes in 1× PBS and blocking for 10-30 minutes in incubation solution (1× PBS, 5% normal goat serum, 1% Triton X-100). Primary antibodies were applied in incubation solution and kept at 4°C overnight with rocking. Following four washes in incubation solution, secondary antibodies were applied in incubation solution and kept at 4°C overnight with rocking. Following four additional washes in incubation solution, the guts were equilibrated in mounting medium (80% glycerol, 100 mM Tris pH 8.5). Intestines were imaged using either an Olympus Fluoview 300 (Olympus America) or a Zeiss LSM 510 META confocal microscope. Images were processed using Adobe PhotoShop v4.0 (Adobe Systems). To detect *Drosophila* V-ATPase subunit B on immunoblots using *Manduca* antibody C23, two third-instar Oregon-R larvae were ground in loading buffer and the protein separated on a 12% polyacrylamide gel, then blotted and probed according to standard protocols.

The authors gratefully acknowledge M. Huss, D. Branton, R. Fehon, J. Sisson and R. Cohen for gifts of antibodies, S. Newfeld for the *mex* promoter fragment, and M. Gonzalez-Gaitan for Rab5 antibodies and the Rab5S43N and myc-2xFYVE fly stocks. We also thank S. Gilroy and R. Cyr for use of their confocal microscope, C. Gay for suggesting the use of Acridine Orange, D. Hess for technical assistance, and D. Cavener for his support. Finally, we thank R. Patterson, E. Siegfried, A. LeBivic and members of the Thomas lab for their critical evaluation of this manuscript. This work was partially funded by NIH grant #GM52506.

References

Ashburner, M. (1989). *Drosophila*: *A Laboratory Handbook.* New York: Cold Spring Harbor Press.

Bement, W. M. and Mooseker, M. S. (1996). The cytoskeleton of the intestinal epithelium. In *The Cytoskeleton* (ed. J. E. Hesketh and I. F. Pryme) Vol. **3**. pp. 359-404. Greenwich: JAI Press.

Bennett, V. and Baines, A. J. (2001). Spectrin and ankyrin-based pathways: metazoan inventions for integrating cells into tissues. *Physiol. Rev.* **81**, 1353-1392.

Bonfati, P., Colombo, A., Heintzelman, M. B., Mooseker, M. S. and Camatini, M. (1992). The molecular architecture of an insect midgut brush border cytoskeleton. *Eur. J. Cell Biol.* **57**, 298-307.

De Matteis, M. A. and Morrow, J. S. (2000). Spectrin tethers and mesh in the biosynthetic pathway. *J. Cell Sci.* **113**, 2331-2343.

Dow, J. A. (1992). pH gradients in lepidopteran midgut. *J. Exp. Biol.* **172**, 355-375.

Dow, J. A. (1999). The multifunctional *Drosophila melanogaster* V-ATPase is encoded by a multigene family. *J. Bioenerg. Biomembr.* **31**, 75-83.

Dow, J. A., Maddrell, S. H., Gortz, A., Skaer, N. J., Brogan, S. and Kaiser, K. (1994). The malpighian tubules of *Drosophila* melanogaster: a novel phenotype for studies of fluid secretion and its control. *J. Exp. Biol.* **197**, 421-428.

Dubreuil, R. R., Frankel, J., Wang, P., Howrylak, J., Kappil, M. and Grushko, T. A. (1998). Mutations of alpha spectrin and labial block cuprophilic cell differentiation and acid secretion in the middle midgut of *Drosophila* larvae. *Dev. Biol.* **194**, 1-11.

Dubreuil, R. R., Wang, P., Dahl, S., Lee, J. and Goldstein, L. S. (2000). *Drosophila*

beta spectrin functions independently of alpha spectrin to polarize the Na,K ATPase in epithelial cells. *J. Cell Biol.* **149**, 647-656.

Dubreuil, R. R., Grushko, T. and Baumann, O. (2001). Differential effects of a labial mutation on the development, structure, and function of stomach acid-secreting cells in *Drosophila melanogaster* larvae and adults. *Cell Tissue Res.* **306**, 167-178.

Filshie, D. K., Pulson, D. F. and Waterhouse, D. F. (1971). Ultrastructure of the copper-accumulating region of the *Drosophila* larval midgut. *Tissue Cell* **3**, 77-102.

Forte, J. G. and Yao, X. (1996). The membrane-recruitment-and-recycling hypothesis of gastric HCl secretion. *Trends Cell Biol.* **6**, 45-48.

Hirokawa, N., Cheney, R. E. and Willard, M. (1983a). Location of a protein of the fodrin-spectrin-TW260/240 family in the mouse intestinal brush border. *Cell* **32**, 953-965.

Hirokawa, N., Keller III, T. S., Chasan, R. and Mooseker, M. (1983b). Mechanism of brush border contractility studied by the quick-freeze, deep-etch method. *J. Cell Biol.* **96**, 1325-1336.

Jankovics, F., Sinka, R. and Erdelyi, M. (2001). An interaction type of genetic screen reveals a role of the Rab11 gene in oskar mRNA localization in the developing *Drosophila melanogaster* oocyte. *Genetics* **158**, 1177-1188.

Kamal, A., Ying, Y. and Anderson, R. G. (1998). Annexin VI-mediated loss of spectrin during coated pit budding is coupled to delivery of LDL to lysosomes. *J. Cell Biol.* **142**, 937-947.

Lee, J. K., Coyne, R. S., Dubreuil, R. R., Goldstein, L. S. and Branton, D. (1993). Cell shape and interaction defects in alpha-spectrin mutants of *Drosophila melanogaster*. *J. Cell Biol.* **123**, 1797-1809.

Medina, E., Williams, J., Klipfell, E., Zarnescu, D., Thomas, C. and Le Bivic, A. (2002). Crumbs interacts with moesin and beta(Heavy)-spectrin in the apical membrane skeleton of *Drosophila*. *J. Cell Biol.* **158**, 941-951.

Merrifield, C. J. (2004). Seeing is believing: imaging actin dynamics at single sites of endocytosis. *Trends Cell Biol.* **14**, 352-358.

Morgan, N. S., Hentzelman, M. B. and Mooseker, M. S. (1995). Characterization of myosin-IA and myosin-IB, two unconventional myosins associated with the *Drosophila* brush border cytoskeleton. *Dev. Biol.* **172**, 51-71.

Newfeld, S. J., Chartoff, E. H., Graff, J. M., Melton, D. A. and Gelbart, W. M. (1996). Mothers against dpp encodes a conserved cytoplasmic protein required in DPP/TGF-beta responsive cells. *Development* **122**, 2099-2108.

Pastor-Soler, N., Beaulieu, V., Litvin, T. N., Da Silva, N., Chen, Y., Brown, D., Buck, J., Levin, L. R. and Breton, S. (2003). Bicarbonate-regulated adenylyl cyclase (sAC) is a sensor that regulates pH-dependent V-ATPase recycling. *J. Biol. Chem.* **278**, 49523-49529.

Pfeffer, S. (2003). Membrane domains in the secretory and endocytic pathways. *Cell* **112**, 507-517.

Raiborg, C., Rusten, T. E. and Stenmark, H. (2003). Protein sorting into multivesicular endosomes. *Curr. Opin. Cell Biol.* **15**, 446-455.

Seabra, M. C. and Wasmeier, C. (2004). Controlling the location and activation of Rab GTPases. *Curr. Opin. Cell Biol.* **16**, 451-457.

Sisson, J. C., Field, C., Ventura, R., Royou, A. and Sullivan, W. (2000). Lava lamp, a novel peripheral golgi protein, is required for *Drosophila melanogaster* cellularization. *J. Cell Biol.* **151**, 905-918.

Stidwill, R. P., Wysolmerski, T. and Burgess, D. R. (1984). The brush border cytoskeleton is not static: in vivo turnover of proteins. *J. Cell Biol.* **98**, 641-645.

Tepass, U. (1997). Epithelial differentiation in *Drosophila*. *BioEssays* **19**, 673-682.

Thomas, C. M. and Kiehart, D. P. (1994). Beta heavy-spectrin has a restricted tissue and subcellular distribution during *Drosophila* embryogenesis. *Development* **120**, 2039-2050

Thomas, C. M., Zarnescu, D. C., Juedes, A. E., Bales, M. A., Londergan, A., Korte, C. C. and Kiehart, D. P. (1998). *Drosophila* beta heavy-spectrin is essential for development and contributes to specific cell fates in the eye. *Development* **125**, 2125-2134.

Wieczorek, H., Grber, G., Harvey, W. R., Huss, M., Merzendorfer, H. and Zeiske, W. (2000). Structure and regulation of insect plasma membrane H(+)V-ATPase. *J. Exp. Biol.* **203**, 127-135.

Williams, J. A., MacIver, B., Klipfell, E. A. and Thomas, C. M. (2004). The C-terminal domain of *Drosophila* (beta) heavy-spectrin exhibits autonomous membrane association and modulates membrane area. *J. Cell Sci.* **117**, 771-782.

Wucherpfennig, T., Wilsch-Brauninger, M. and Gonzalez-Gaitan, M. (2003). Role of *Drosophila* Rab5 during endosomal trafficking at the synapse and evoked neurotransmitter release. *J. Cell Biol.* **161**, 609-624.

Zarnescu, D. C. and Thomas, C. M. (1999). Apical spectrin is essential for epithelial morphogenesis but not apicobasal polarity in *Drosophila*. *J. Cell Biol.* **146**, 1075-1086.